PHYSICAL REVIEW B **92**, 161201(R) (2015)

Modulation of ferromagnetism in (In,Fe)As quantum wells via electrically controlled deformation of the electron wave functions

Le Duc Anh,[1] Pham Nam Hai,[1,2] Yuichi Kasahara,[3] Yoshihiro Iwasa,[3,4] and Masaaki Tanaka[1,*]

[1]*Department of Electrical Engineering and Information Systems, The University of Tokyo, 7-3-1 Hongo, Bunkyo-ku, Tokyo 113-8656, Japan*

[2]*Department of Physical Electronics, Tokyo Institute of Technology, 2-12-1 Ookayama, Meguro-ku, Tokyo 152-0033, Japan*

[3]*QPEC and Department of Applied Physics, The University of Tokyo, 7-3-1 Hongo, Bunkyo-ku, Tokyo 113-8656, Japan*

[4]*RIKEN Center for Emergent Matter Science, Wako 351-0198, Japan*

(Received 7 October 2014; revised manuscript received 4 September 2015; published 1 October 2015)

We demonstrate electrical control of ferromagnetism in field-effect transistors with a trilayer quantum well (QW) channel containing an ultrathin *n-type* ferromagnetic semiconductor (In,Fe)As layer. A gate voltage is applied to control the electron wave functions φ_i in the QW, such that the overlap of φ_i and the (In,Fe)As layer is modified. The Curie temperature is largely changed by 42%, whereas the change in sheet carrier concentration is two to three orders of magnitude smaller than that of previous gating experiments. This result provides an approach for versatile, low power, and ultrafast manipulation of magnetization.

DOI: 10.1103/PhysRevB.92.161201 PACS number(s): 75.50.Pp, 75.75.−c, 75.78.Jp

Recently, the change of magnetic properties using an external gate voltage in field-effect transistor (FET) structure was demonstrated in carrier-induced ferromagnetic semiconductors (FMSs) [1–8] and ferromagnetic ultrathin metal films [9–14], which is expected to reduce the power consumption of spin devices. Commonly in these experiments, although the ferromagnetic channels are very thin (<5 nm), the two-dimensional (2D) quantization is smeared out because of the carriers' low coherency. The Curie temperature (T_C) of these thin films monotonically depends on the carrier density n, which is varied by the effect of electrical gating, as predicted for three-dimensional (3D) ferromagnets [1–3]. A very large change in the sheet carrier density n_{sheet}(Δn_{sheet} = 10^{13}–10^{14}cm^{-2}) is typically required to generate a pronounced change in the magnetic properties, which in practice is difficult, and consumes a lot of energy ($E \propto \Delta n_{sheet}^2$). Furthermore, the response time is limited by the device's capacitance and the carriers' transit time from outside electrodes to the channel, which is at shortest picoseconds.

In 2D ferromagnetic systems such as FMS quantum wells (QWs), however, the physics is different, as illustrated in the top panel of Fig. 1(a): Due to the quantization of the density of states, T_C does not change with the carrier density unless the Fermi level has reached the next subband [15]. Instead, theoretical studies suggested that T_C is very sensitive to the shape of the carrier wave function $\varphi_i(z)$ of the occupied subband i, as described by the equation $T_C \propto \sum_i \int_{FMS} |\varphi_i(z)|^4 dz$ [16–19], where z is the direction normal to the interface and the integral is performed inside the ferromagnetic layer in the QW (the fourth power is of great importance because it does *not* represent the carrier density, which is the square of the wave function, but represents the distribution of carriers in the ferromagnetic layer). Therefore, as illustrated in the bottom panel of Fig. 1(a), by using the gate voltage (V_G) to deform the shape of the wave functions φ_i of the QW, one can effectively control the magnetic properties *without the need of changing the carrier concentration*. This method has two important advantages over the conventional method: First, since no extra charge is needed, the charging energy of the FET's capacitor, which determines the power consumption for modulating magnetization, can be greatly reduced. Second, instead of traveling hundreds of nanometer-long paths as in the conventional method, electron carriers are redistributed over only a few nanometers in the QW. Therefore, the modulation speed can be as fast as ∼100 fs [20,21]. Another feature of this method is the ability to tune the relation between T_C and V_G at will by specifying the appropriate position and thickness of the ferromagnetic layer inside the QW [16–18]. However, experimental demonstration of such functionality has never been reported due to the lack of a good ferromagnetic QW so far.

Here we demonstrate such a control of ferromagnetism of 2D ferromagnetic QW via deforming the carrier wave function, using electrical gating in a FET structure. The system used in this study is a semiconductor InAs-based QW that contains a thin *n*-type FMS (In,Fe)As layer. Among the many types of FMSs, (In,Fe)As is unique and promising because it is the only reliable *n*-type FMS among III-V based semiconductors [22]. In this material, Fe atoms in the trivalent state Fe^{3+} replace In atoms and thus play only the role of local magnetic moments. Electron carriers, which are independently supplied by defects or donors, interact strongly with these local Fe magnetic moments through the *s-d* exchange interaction to induce ferromagnetism with a T_C of up to several tens of Kelvin with a modest electron density (∼6×10^{18}cm^{-3}), and there is plenty of room for improvement [19,22–26]. We have observed that the electron carriers in (In,Fe)As reside in the conduction band and exhibit high coherency [19,24]. In fact, magnetic circular dichroism (MCD) spectroscopy has confirmed the quantum size effect (QSE) in QWs consisting of InAs/(In,Fe)As/InAs trilayers with a total thickness as large as 40 nm, in which the electron wave functions smoothly extend throughout the trilayers [19,25]. These features of the *n*-type FMS (In,Fe)As make it possible to demonstrate the electrical control of ferromagnetism via wave function manipulation.

We prepared a QW structure (sample A) consisting of InAs (2 nm)/($In_{0.94}$,$Fe_{0.06}$)As(8 nm)/InAs(5 nm) on an AlSb buffer, all grown on a semi-insulating GaAs (001) substrate by molecular beam epitaxy [left panel in Fig. 1(b)] [27]. Because of the large conduction-band offset at the bottom

*Corresponding author: masaaki@ee.t.u-tokyo.ac.jp

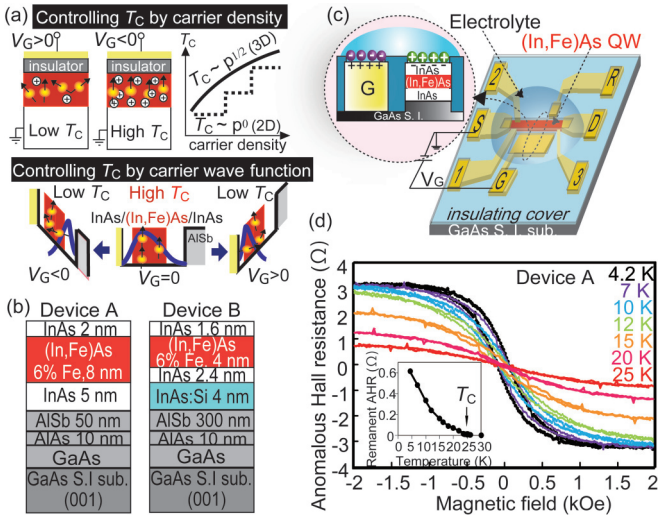

FIG. 1. (Color) (a) Schematic illustration of the two methods: Controlling T_C by carrier density as in previous works (top panel) and by carrier wave function as in the present study (bottom panel). Unlike 3D cases, in ferromagnetic QW, T_C does not change monotonically with the carrier density, which is due to the steplike change of the density of states. (b) Sample structures of device A (left panel) and device B (right panel). In both samples, the QW is the top $InAs/(In_{0.94},Fe_{0.06})As/InAs$ trilayer structure. The Fe concentration is fixed at 6%. In device B, the bottom 5-nm InAs layer in the QW is doped with Si(5×10^{18}cm^{-3}). (c) Schematic structure of the FET device with electrolyte (DEME-TFSI) between the gate (G), the reference electrode (R), and the trilayer QW. The source (S) and drain (D) electrodes and the electrodes numbered 1, 2, and 3 are used for transport measurements. (d) Anomalous Hall resistance (AHR) of device A at various temperatures. The inset shows the temperature dependence of the remanent AHR, which indicates a T_C of 24 K.

InAs/AlSb interface (1.35 eV) [28], the electrons are confined to the top InAs/(In,Fe)As/InAs trilayer and form quantized electronic states. The QSE is evident in the blue shift of the MCD spectrum of sample A [27]. We used an electric-double-layer-type FET structure to control the carrier wave functions in the magnetic trilayer QWs, as illustrated in Fig. 1(c). The sample was etched into a $50 \times 200\ \mu$m^2 Hall bar using standard photolithography and ion milling. A side-gate electrode (G), a reference electrode (R), and several electrodes (source S, drain D, and electrodes numbered 1–3) for transport measurements were formed via the electron-beam evaporation and lift-off of an Au(50 nm)/Cr(5 nm) film. The side-gate pad (G), the reference pad (R), and the (In,Fe)As channel were covered with electrolyte [N,N-diethyl-N-methyl-N-(2-methoxyethyl)ammonium bis (trifluoromethylsulfonyl) imide, DEME-TFSI] to form the FET structure. Other regions of the device were separated from the electrolyte by an insulating resist. As illustrated in the inset of Fig. 1(c), when a positive V_G is applied, ions in the electrolyte accumulate at the surface of the semiconductor channel and form an electric-double-layer capacitor, which changes the potential and electron density in the InAs/(In,Fe)As/InAs trilayer QW.

The transport and magnetic properties of the trilayer QW were characterized by Hall measurements [27]. The Hall resistance of (In,Fe)As always consists of a large n-type normal

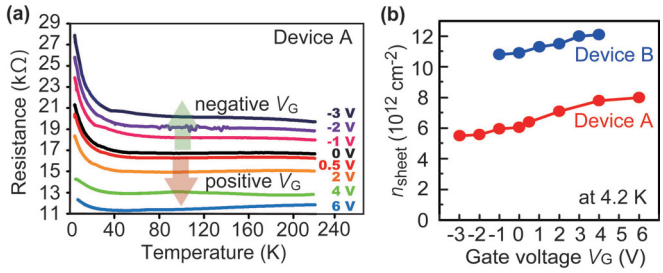

FIG. 2. (Color online) (a) Temperature dependence of the R_{13} of device A at various gate voltage V_G values. (b) n_{sheet} values of device A (red circles) and device B (blue circles) at 4.2 K as functions of V_G.

Hall resistance (NHR) and a much smaller anomalous Hall resistance (AHR) that is proportional to the magnetization. The small AHR (~3% of the total Hall resistance) can be obtained by subtracting the negative slope of the NHR at a high magnetic field (1 T) from the raw Hall-resistance data. The large contribution of the NHR in the Hall-resistance data allows us to accurately estimate the electron density from the Hall measurements. T_C was estimated by monitoring the temperature dependence of the remanent AHR. Figure 1(d) presents the AHR of the trilayer QW in device A at $V_G = 0$ V at various temperatures, in which clear ferromagnetic hysteresis is observed at low temperatures. The inset presents the remanent AHR vs temperature T, indicating a T_C of 24 K.

Figure 2(a) shows the temperature dependence of the resistance (R-T) measured between terminals 1 and 3 of device A(R_{13}) using a four-terminal method. R_{13} systematically decreases (increases) when a positive (negative) V_G is applied, as expected. Figure 2(b) shows n_{sheet} in the InAs/(In,Fe)As/InAs trilayer QW at various V_G values estimated by Hall measurements at 4.2 K. The n_{sheet} of device A (red circles) changes from 6.06×10^{12}cm^{-2} (at $V_G = 0$ V) to 8×10^{12}cm^{-2} (at $V_G = 6$ V) or to 5.52×10^{12}cm^{-2} (at $V_G = -3$ V). The Δn_{sheet} is small, probably because of the existence of a large number of surface states at the top InAs layer, which tends to pin the Fermi level.

Figures 3(a) and 3(c) show the evolution of the AHR of device A at 15 K when V_G is adjusted as follows: 0 V → 0.5 V → 6 V → 0 V and 0 V → −3 V → 0 V, respectively. At $V_G = 6$ and −3 V, the hysteresis in the AHR-H characteristics almost disappears, whereas it recovers after V_G is returned to 0. These results demonstrate that the ferromagnetism of the (In,Fe)As thin film can be reversibly controlled by electrical gating. Figures 3(b) and 3(d) show the remanent AHR vs T of device A at various positive and negative V_G values, respectively, and illustrate the evolution of T_C. As summarized in Fig. 4(a), the T_C of the (In,Fe)As layer of device A (black circles) decreases from its initial value of 24 K($V_G = 0$ V) to 17 K($V_G = 6$ V) or 14 K($V_G = -3$ V).

Compared with previous electrical-gating experiments [1–14], the present results for device A exhibit two distinct features. First, very effective control of T_C is realized (the largest change in T_C, $\Delta T_C/T_C = [T_C(V_G) - T_C(0)]/T_C(0)$, is −42% at $V_G = -3$ V) despite a very small change in n_{sheet} (the corresponding $\Delta n_{sheet} = -5.4 \times 10^{11}$cm^{-2}). This Δn_{sheet} is two to three orders of magnitude smaller than the change of the n_{sheet} that was required in almost all the previous gating

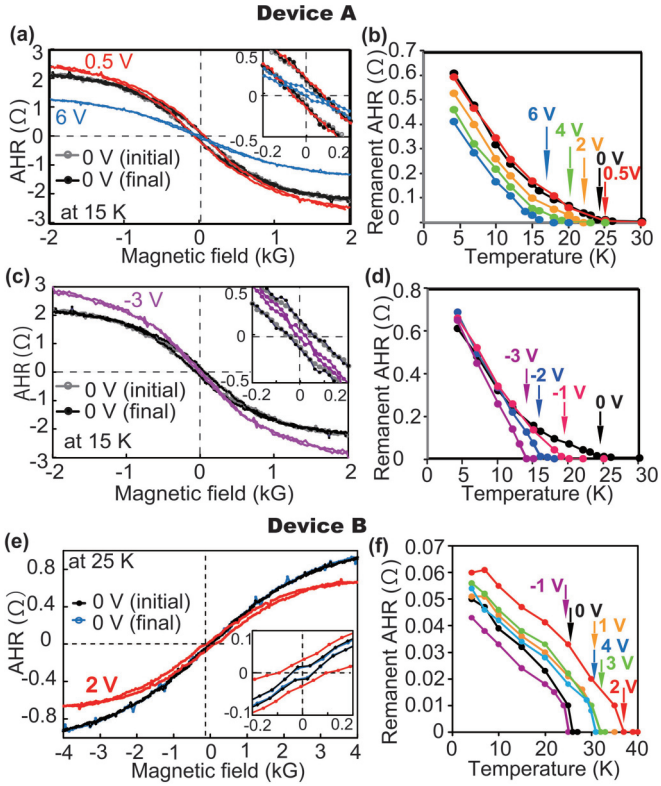

FIG. 3. (Color) (a), (c) Evolution of the AHR of device A measured at 15 K when adjusting V_G as follows: 0 V → 0.5 V → 6 V → 0 V and 0 V → −3 V → 0 V, respectively. The insets present the AHR data near the origin, which exhibit clear changes in hysteresis characteristics. (b), (d) Temperature dependence of the remanent AHR of device A at various V_G values. The colored arrows indicate the T_C values of device A at each V_G. (e) Evolution of the AHR of device B measured at 25 K when adjusting V_G: 0 V → 2 V → 0 V. The inset presents the AHR data near the origin. (f) Temperature dependence of the remanent AHR of device B at various V_G values. The colored arrows indicate the T_C values of device B at each V_G.

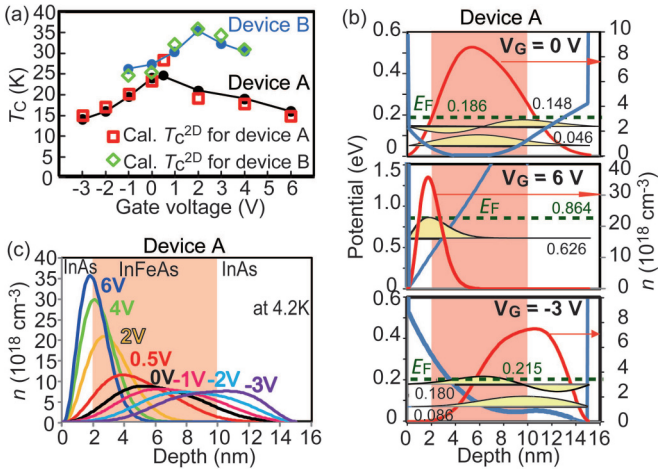

FIG. 4. (Color online) (a) Experimental T_C values of device A (black circles) and device B (blue circles), respectively, as functions of V_G. Red squares and green diamonds represent the T_C^{2D} values calculated using the 2D mean-field Zener model for device A and B, respectively, which exhibit good agreement with the experimental results. (b) Calculated potential profiles (blue curves), electron wave functions (yellow shapes), and electron-density distributions (red curves, with arrows pointing to the corresponding right-hand vertical axes) of the QW of device A at $V_G = 0$,6, and −3 V, from top to bottom. The Fermi levels (green dashed lines) and quantized energy levels (black lines, in the eV unit) in the trilayer QWs are shown. (c) Calculated evolution of the electron-density distribution in the trilayer QW of device A at 4.2 K when V_G is varied from −3 V to 6 V. The reddish regions correspond to the (In,Fe)As layer.

experiments (the only exceptions whose Δn_{sheet} are comparable with the present study are CdMnTe QW [6] and GeMn quantum dots [7], in which, however, the ferromagnetism was turned off by depleting carriers in the ferromagnetic channels). This means that the energy for charging the ferromagnetic channel is dramatically reduced by a factor of 10^{-4}–10^{-6} while maintaining the same effect of modulating the ferromagnetism. Second, T_C varies nonmonotonically with n_{sheet}, reaching a maximum near $V_G = 0.5$ V and decreasing at both positive and negative V_G. This is characteristic of 2D FMS QWs, in which the overlap of the electron wave functions and the (In,Fe)As layer determines the single T_C value of the entire system. Figure 4(b) presents the changes in the potential profile (blue curves) and the electron wave functions (yellow shapes) of the QW in device A at $V_G = 0$, 6, and −3 V, which were obtained through self-consistent calculations [27]. The calculated electron-density distribution in the QW versus V_G is summarized in Fig. 4(c). The integral of the electron-density distribution over the entire QW yields n_{sheet}. The overlap of the wave functions and the local Fe magnetic moments in the (In,Fe)As layer is largest at $V_G = 0.5$ V and decreases as the wave functions move towards the ends of the trilayer QW at both positive and negative V_G, leading to the observed behavior of T_C. These results clearly indicate the feasibility of controlling the ferromagnetism via wave function manipulation and confirm the intrinsic electron-induced ferromagnetism of n-type FMS (In,Fe)As.

In a 2D FMS structure, T_C is given by [16,17,19]

$$T_C^{2D} = \frac{S(S+1)}{12} \frac{A_F^{2D} J_{sd}^2}{k_B} \frac{m^*}{\pi \hbar^2} N_{Fe} \sum_{E_i < E_F} \int_{(In,Fe)As} |\varphi_i(z)|^4 dz. \quad (1)$$

Here, z is the growth direction, S is the spin angular momentum of an Fe atom (=5/2), m^* is the effective electron mass at the Γ point, k_B is the Boltzmann constant, J_{sd} is the s-d exchange interaction, A_F^{2D} is the Stoner enhancement factor in 2D structures [29], and N_{Fe} is the Fe atom density. The calculated T_C^{2D} values [red squares in Fig. 4(a)] exhibit good agreement with the experimental results. It is worth noting that a semiclassical approach based on a modified 3D mean-field Zener model, in which the QSE is ignored, cannot explain the behavior of T_C observed in the present experiment [27]. From the calculations of T_C^{2D}, the effective s-d exchange interaction energy $N_0\alpha$ of the (In,Fe)As QW was estimated to be 3.6 eV. This effective $N_0\alpha$ value was calculated from the value of $(A_F^{2D})^{1/2} J_{sd}$, which implicitly includes the enhancement effect associated with electron-electron interactions in 2D structures.

Finally, we demonstrate the ability to control the relation between T_C and V_G by modifying the QW structure.

Another sample and its corresponding FET device were prepared (device B) using the same procedure but a modified QW structure: InAs(1.6 nm)/($In_{0.94}$,$Fe_{0.06}$)As (4 nm)/InAs (2.4 nm)/Si-doped InAs(4 nm) [right panel of Fig. 1(b)]. Si donors (5×10^{18}cm^{-3}) in the bottom 4-nm InAs layer supply electrons to the QW and attract the 2D electron wave functions towards the bottom AlSb side. This feature, together with the reduced thickness (4 nm) of the (In,Fe)As layer, creates a situation in which the wave functions and Fe magnetic moments are separated when $V_G = 0$; however, their overlap increases as a positive V_G is applied. As shown in Fig. 2(b), device B exhibits a higher n_{sheet} (1.08×10^{13} cm^{-2} at $V_G = 0$) than device A but a weak dependence of n_{sheet} on V_G, similar to device A. Figure 3(e) shows the evolution of the AHR-H characteristics of device B at 25 K for $V_G = 0\,V \rightarrow 2\,V \rightarrow 0\,V$, and Fig. 3(f) summarizes the remanent AHR vs T curves at various V_G values. The sign of AHR in device B is positive, which is opposite to that of device A. The QWs in devices A and B are different in the inversion asymmetry (due to the space charge potential of activated Si donors in device B) and n_{sheet}, both of which could be the origin of the different AHR sign [30,31]. Positive AHR has also been observed in bulklike (In,Fe)As samples doped with Be that have high electron density [22]. Thus, at this stage we suggest that the sign change of AHR is probably due to the difference in n_{sheet}, although a more elaborate study is needed to clarify the mechanism. As can be seen in Fig. 3(e), unlike device A, the ferromagnetism of the (In,Fe)As layer in device B is enhanced by applying positive V_G, as expected, and T_C increases from 27 K (at $V_G = 0\,V$) to a maximum of 35 K (at $V_G = 2\,V$) or to 30 K (at $V_G = 4\,V$), as illustrated in Fig. 4(a) (blue circles). The T_C values calculated by the 2D mean-field Zener model for device B are plotted as green diamonds, which also show good agreement with the experimental values (see Ref. [27] for details of the calculations). Thus, using the appropriate QW structure, one can either increase or decrease the T_C of the (In,Fe)As layer in QWs with the same device configuration. This high degree of freedom in controlling the ferromagnetism is an important advantage, which is attractive for device applications.

In summary, we have demonstrated the electrical control of ferromagnetism in (In,Fe)As QWs by manipulating the overlap between the 2D wave functions and the (In,Fe)As layer. The T_C was largely changed by 10 K ($\Delta T_C/T_C = 42\%$), whereas the change in n_{sheet} is two to three orders of magnitude smaller than that of previous gating experiments. The behavior of T_C was quantitatively explained by the mean-field Zener model for FMS QWs. We have also demonstrated the ability to customize the T_C-V_G relation by modifying the QW structure. These results confirm the intrinsic electron-induced ferromagnetism of n-type FMS (In,Fe)As and open up possibilities of using this material in spintronic devices, as well as provide an approach for versatile, low power, and ultrafast manipulation of magnetization.

This work was partially supported by Grants-in-Aid for Scientific Research (Grants No. 23000010, No. 25000003, No. 2474022, and No. 257388), including the Specially Promoted Research, the Project for Developing Innovation Systems of MEXT, and the Strategic International Collaboration Research Program (SICORP-LEMSUPER) from JST. L.D.A. acknowledges the support from the JSPS Fellowship for Young Scientists and the Program for Leading Graduate Schools (MERIT). P.N.H acknowledges support from the Yazaki Memorial Foundation for Science and Technology, the Murata Science Foundation, and the Toray Science Foundation.

[1] H. Ohno, D. Chiba, F. Matsukura, T. Omiya, E. Abe, T. Dietl, Y. Ohno, and K. Ohtani, Nature (London) **408**, 944 (2000).

[2] D. Chiba, M. Yamanouchi, F. Matsukura, and H. Ohno, Science **301**, 943 (2003).

[3] D. Chiba, F. Matsukura, and H. Ohno, Appl. Phys. Lett. **89**, 162505 (2006).

[4] I. Stolichnov, S. W. E. Riester, H. J. Trodahl, N. Setter, A. W. Rushforth, K. W. Edmonds, R. P. Campion, C. T. Foxon, B. L. Gallagher, and T. Jungwirth, Nat. Mater. **7**, 464 (2008).

[5] M. Sawicki, D. Chiba, A. Korbecka, Y. Nishitani, J. A. Majewski, F. Matsukura, T. Dietl, and H. Ohno, Nat. Phys. **6**, 22 (2010).

[6] H. Boukari, P. Kossacki, M. Bertolini, D. Ferrand, J. Cibert, S. Tatarenko, A. Wasiela, J. A. Gaj, and T. Dietl, Phys. Rev. Lett. **88**, 207204 (2002).

[7] F. Xiu, Y. Wang, J. Kim, A. Hong, J. Tang, A. P. Jacob, J. Zou, and K. L. Wang, Nat. Mater. **9**, 337 (2010).

[8] Y. Yamada, K. Ueno, T. Fukumura, H. T. Yuan, H. Shimotani, Y. Iwasa, L. Gu, S. Tsukimoto, Y. Ikuhara, and M. Kawasaki, Science **332**, 1065 (2011).

[9] M. Weisheit, S. Fähler, A. Marty, Y. Souche, C. Poinsignon, and D. Givord, Science **315**, 349 (2007).

[10] T. Maruyama, Y. Shiota, T. Nozaki, K. Ohta, N. Toda, M. Mizuguchi, A. A. Tulapurkar, T. Shinjo, M. Shiraishi, S. Mizukami, Y. Ando, and Y. Suzuki, Nat. Nanotechnol. **4**, 158 (2009).

[11] T. Seki, M. Kohda, J. Nitta, and K. Takanashi, Appl. Phys. Lett. **98**, 212505 (2011).

[12] D. Chiba, S. Fukami, K. Shimamura, N. Ishiwata, K. Kobayashi, and T. Ono, Nat. Mater. **10**, 853 (2011).

[13] M. Endo, S. Kanai, S. Ikeda, F. Matsukura, and H. Ohno, Appl. Phys. Lett. **96**, 212503 (2010).

[14] M. Zhernenkov, M. R. Fitzsimmons, J. Chlistunoff, J. Majewski, I. Tudosa, and E. E. Fullerton, Phys. Rev. B **82**, 024420 (2010).

[15] N. Kim, J. W. Kim, S. J. Lee, Y. Shon, T. W. Kang, G. Ihm, and T. F. George, J. Supercond.: Novel Magn.**18**, 189 (2005).

[16] B. Lee, T. Jungwirth, and A. H. MacDonald, Semicond. Sci. Technol. **17**, 393 (2002).

[17] B. Lee, T. Jungwirth, and A. H. MacDonald, Phys. Rev. B **61**, 15606 (2000).

[18] E. Dias Cabral, M. A. Boselli, R. Oszwaldowski, I. Žutić, and I. C. da Cunha Lima, Phys. Rev. B **84**, 085315 (2011).

[19] L. D. Anh, P. N. Hai, and M. Tanaka, Appl. Phys. Lett. **104**, 046404 (2014).
[20] H. Sakaki, Jpn. J. Appl. Phys. **21**, L381 (1982).
[21] K. Hirakawa, H. Sakaki, and J. Yoshino, Phys. Rev. Lett. **54**, 1279 (1985).
[22] P. N. Hai, L. D. Anh, S. Mohan, T. Tamegai, M. Kodzuka, T. Ohkubo, K. Hono, and M. Tanaka, Appl. Phys. Lett. **101**, 182403 (2012).
[23] P. N. Hai, D. Sasaki, L. D. Anh, and M. Tanaka, Appl. Phys. Lett. **100**, 262409 (2012).
[24] P. N. Hai, L. D. Anh, and M. Tanaka, Appl. Phys. Lett. **101**, 252410 (2012).
[25] D. Sasaki, L. D. Anh, P. N. Hai, and M. Tanaka, Appl. Phys. Lett. **104**, 142406 (2014).
[26] M. Tanaka, S. Ohya, and P. N. Hai, Appl. Phys. Rev. **1**, 011102 (2014).
[27] See Supplemental Material at http://link.aps.org/supplemental/10.1103/PhysRevB.92.161201 for details of methods and supplementary data.
[28] A. Nakagawa, H. Kroemer, and J. H. English, Appl. Phys. Lett. **54**, 1893 (1989).
[29] T. Dietl, A. Haury, and Y. M. d'Aubigne, Phys. Rev. B **55**, R3347 (1997).
[30] D. Chiba, A. Werpachowska, M. Endo, Y. Nishitani, F. Matsukura, T. Dietl, and H. Ohno, Phys. Rev. Lett. **104**, 106601 (2010).
[31] K. S. Takahashi, M. Onoda, M. Kawasaki, N. Nagaosa, and Y. Tokura, Phys. Rev. Lett. **103**, 057204 (2009).